Supplemental Material for "N-Phonon Bundle Emission via the Stokes Process"

Qian Bin,[1] Xin-You Lü,[1,*] Fabrice P. Laussy,[2,3] Franco Nori,[4,5] and Ying Wu[1,†]

[1]*School of Physics, Huazhong University of Science and Technology, Wuhan, 430074, P. R. China*
[2]*Faculty of Science and Engineering, University of Wolverhampton, Wulfruna Street, Wolverhampton WV1 1LY, United Kingdom*
[3]*Russian Quantum Center, Novaya 100, 143025 Skolkovo, Moscow Region, Russia*
[4]*Theoretical Quantum Physics Laboratory, RIKEN Cluster for Pioneering Research, Wako-shi, Saitama 351-0198, Japan*
[5]*Physics Department, The university of Michigan, Ann Arbor, Michgan 48109-1040, USA*

(Dated: January 12, 2020)

This supplementary material contains five parts: I. The detailed derivation of the super-Rabi oscillation frequencies that arise from the Stokes resonances in the three parameter regimes considered in the main text; II. In the two-phonon emission regime, we present a long-time quantum trajectory and a small-time counterpart featuring an undesired 2×2-phonon bundle emission, together with a detailed discussion of the actual cascade emission processes. A tiny fraction of the quantum trajectory under the condition of three-phonon resonance shows the process of three-phonon bundle emission. III. A discussion of the purity of high-order (four- and five-phonon) emission; IV. A discussion of the effect of pure dephasing on the purities of n-phonon emission, and conditions for optimum n-phonon bundle emission; V. Quantum correlations of n-phonon bundles and the various regimes of emission, from single-bundle emission to n-phonon lasers.

DERIVATION OF THE N-PHONON TRANSITION RATES

We remind the system Hamiltonian ($\hbar = 1$)

$$H = \omega_b b^\dagger b + \omega_\sigma \sigma^\dagger \sigma + \lambda \sigma^\dagger \sigma (b^\dagger + b) + \Omega \left(e^{i\omega_L t}\ \sigma + e^{-i\omega_L t}\ \sigma^\dagger \right). \tag{S1}$$

In a frame rotating with the laser at frequency ω_L, Eq. (S1) becomes

$$H = \omega_b b^\dagger b + \Delta \sigma^\dagger \sigma + \lambda \sigma^\dagger \sigma (b^\dagger + b) + \Omega \left(\sigma + \sigma^\dagger \right). \tag{S2}$$

In the following, we address in turn the three regimes of interest discussed in the text.

Low-driving and weak-coupling regime

In the parameter regime $\Omega, \lambda \ll \omega_b$, the eigenstates of the above Hamiltonian are close to the product states $|n, c/v\rangle$. When the QD is driven at a n-phonon assisted Stokes resonance $\Delta = \omega_\sigma - \omega_L = -n\omega_b$, one can consider the truncated Hilbert space spanned by the $2(n+1)$ product states $\{|0, v\rangle,\ |n, c\rangle,\ |0, c\rangle,\ |1, v\rangle,\ \cdots,\ |n-1, c\rangle,\ |n, v\rangle\}$ [1, 2]. The matrix form of the reduced Hamiltonian then reads

$$H^{(n)} = \begin{pmatrix} \mathcal{H}^{(n)} & \mathcal{X}^{(n)} \\ \mathcal{X}^{(n)\mathrm{T}} & \mathcal{R}^{(n)} \end{pmatrix}, \tag{S3}$$

where $\mathcal{H}^{(n)}$ corresponds to the subspace $\{|0, v\rangle,\ |n, c\rangle\}$, with

$$\mathcal{H}^{(n)} = \begin{pmatrix} 0 & 0 \\ 0 & 0 \end{pmatrix} \tag{S4}$$

and $\mathcal{R}^{(n)}$ corresponds to the remaining subspace of the Hamiltonian matrix $H^{(n)}$. The two subspaces $\mathcal{H}^{(n)}$ and $\mathcal{R}^{(n)}$ are coupled by $\mathcal{X}^{(n)}$, which is a $2 \times 2n$ matrix of the type

$$\mathcal{X}^{(n)} = \begin{pmatrix} \Omega & 0 & \cdots & 0 & 0 \\ 0 & 0 & \cdots & \sqrt{n}\lambda & \Omega \end{pmatrix}. \tag{S5}$$

By applying matrix perturbation theory, we can derive

$$\mathcal{H}_{\mathrm{eff}}^{(n)} = \mathcal{H}^{(n)} + \mathcal{X}^{(n)} (-\mathcal{R}^{(n)})^{-1} \mathcal{X}^{(n)\mathrm{T}} \tag{S6}$$

to adiabatically eliminate the intermediate states $\{|0,c\rangle, |1,v\rangle, \cdots, |n-1,c\rangle, |n,v\rangle\}$. This provides an effective system Hamiltonian in the subspace $\{|0,v\rangle, |n,c\rangle\}$ whose off-diagonal elements describe the effective n-phonon super-Rabi frequency between the states $|0,v\rangle$ and $|n,c\rangle$, i.e., $\Omega_{\rm eff}^{(n)} = \mathcal{H}_{\rm eff}^{(n)}(1,2) = \mathcal{H}_{\rm eff}^{(n)}(2,1)$. This calculation, involving the $2(n+1)$ product states, can be used to obtain analytical expressions of $\Omega_{\rm eff}^{(n)}$ for small n, but it is too cumbersome for larger n. To calculate the general expression of $\Omega_{\rm eff}^{(n)}$ with perturbation theory, we first consider the truncated Hilbert space spanned by the product states $\{|0,v\rangle, |n,c\rangle, |n-1,c\rangle, |n,v\rangle\}$. The matrix form of the reduced Hamiltonian then reads

$$H^{(n)} = \begin{pmatrix} 0 & 0 & \Omega_{\rm eff}^{(n-1)} & 0 \\ 0 & \Delta + n\omega_b & \sqrt{n}\lambda & \Omega \\ \Omega_{\rm eff}^{(n-1)} & \sqrt{n}\lambda & \Delta + (n-1)\omega_b & 0 \\ 0 & \Omega & 0 & n\omega_b \end{pmatrix} = \begin{pmatrix} \mathcal{H}^{(n)} & \mathcal{X}^{(n)} \\ \mathcal{X}^{(n)\rm T} & \mathcal{R}^{(n)} \end{pmatrix}, \quad \mathcal{X}^{(n)} = \begin{pmatrix} \Omega_{\rm eff}^{(n-1)} & 0 \\ \sqrt{n}\lambda & \Omega \end{pmatrix}, \tag{S7}$$

where $\Omega_{\rm eff}^{(n-1)}$ is the effective coupling between the states $|0,v\rangle$ and $|n-1,c\rangle$. By applying Eq. (S6), we obtain

$$\Omega_{\rm eff}^{(n)} = \mathcal{H}_{\rm eff}^{(n)}(1,2) = \mathcal{H}_{\rm eff}^{(n)}(2,1) = -\frac{\sqrt{n}\lambda}{\Delta + (n-1)\omega_b}\Omega_{\rm eff}^{(n-1)}. \tag{S8}$$

Following the same procedure, we find

$$\Omega_{\rm eff}^{(n-1)} = -\frac{\sqrt{n-1}\lambda}{\Delta + (n-2)\omega_b}\Omega_{\rm eff}^{(n-2)} = (-1)^{(n-1)}\frac{\sqrt{n-1}\lambda}{\Delta + (n-2)\omega_b}\frac{\sqrt{n-2}\lambda}{\Delta + (n-3)\omega_b}\cdots\frac{\sqrt{2}\lambda}{\Delta + \omega_b}\Omega_{\rm eff}^{(1)}. \tag{S9}$$

We now consider the truncated Hilbert space spanned by the product states $\{|0,v\rangle, |1,c\rangle, |0,c\rangle, |1,v\rangle\}$, and then the reduced Hamiltonian reads

$$H^{(1)} = \begin{pmatrix} 0 & 0 & \Omega & 0 \\ 0 & \Delta + \omega_b & \lambda & \Omega \\ \Omega & \lambda & \Delta & 0 \\ 0 & \Omega & 0 & \omega_b \end{pmatrix} = \begin{pmatrix} \mathcal{H}^{(1)} & \mathcal{X}^{(1)} \\ \mathcal{X}^{(1)\rm T} & \mathcal{R}^{(1)} \end{pmatrix}, \quad \mathcal{X}^{(1)} = \begin{pmatrix} \Omega & 0 \\ \lambda & \Omega \end{pmatrix}. \tag{S10}$$

By applying Eq. (S6), we obtain $\Omega_{\rm eff}^{(1)} = \mathcal{H}_{\rm eff}^{(1)}(1,2) = \mathcal{H}_{\rm eff}^{(1)}(2,1) = -\Omega\lambda/\Delta$. For the n-phonon resonance, i.e., $\Delta = \omega_\sigma - \omega_L = -n\omega_b$, the effective n-phonon super-Rabi frequency up to any order can be obtained analytically as

$$\Omega_{\rm eff}^{(n)} = -\frac{\sqrt{n}\lambda}{\Delta + (n-1)\omega_b}\Omega_{\rm eff}^{(n-1)} = (-1)^n\frac{\sqrt{n}\lambda}{\Delta + (n-1)\omega_b}\frac{\sqrt{n-1}\lambda}{\Delta + (n-2)\omega_b}\cdots\frac{\sqrt{2}\lambda}{\Delta + \omega_b}\frac{\lambda\Omega}{\Delta} = \left(\frac{\lambda}{\omega_b}\right)^n\frac{\Omega}{\sqrt{n!}}. \tag{S11}$$

In the main text, it is shown that sinusoidal oscillations at the rate $\Omega_{\rm eff}^{(n)}$ give a very good numerical agreement with the full-numerical simulations, that involve small residual couplings to all manifolds. The system's state populations are found from $P_{jk}(t) = |\langle j,k|\psi(t)\rangle|^2$ ($j = n$ and $k = c, v$) and the phonon population is well approximated by $P_n(t) \approx P_{nc}(t)$ with $P_n(t) = |\langle n|\psi_b(t)\rangle|^2$, with $P_n(t) = \langle n|\rho_b(t)|n\rangle$, where $\rho_b(t)$ is the state of the system after tracing out the QD degrees of freedom.

Strong-coupling regime

In the parameter regime $\lambda \sim \omega_b$, the strong electron-phonon coupling changes the energy-levels structure, giving rise to different n-phonon assisted Stokes resonance conditions. In this case, rather than the adiabatic elimination described in the previous section, it is simpler to first apply a displaced transformation $H \to DHD^\dagger$, with $D = \exp\left[(\lambda/\omega_b)\sigma^\dagger\sigma(b^\dagger - b)\right]$. The system Hamiltonian then becomes

$$H = \omega_b b^\dagger b + \tilde{\omega}_\sigma\sigma^\dagger\sigma + \Omega\left\{\exp\left(-i\omega_L t\right)\sigma^\dagger\exp\left[\lambda\left(b^\dagger - b\right)/\omega_b\right] + \text{H.c.}\right\}, \tag{S12}$$

where $\tilde{\omega}_\sigma = \omega_\sigma - \lambda^2/\omega_b$ is the reduced flip frequency of the QD. The third term in Eq. (S12) can be further developed as [3]

$$H_{\rm int} = \Omega\exp(-i\omega_L t)\exp\left[-\frac{1}{2}\left(\frac{\lambda}{\omega_b}\right)^2\right]\sigma^\dagger\sum_{k=0}^{\infty}\left(\frac{\lambda}{\omega_b}\right)^k\frac{b^{\dagger k}}{k!}\sum_{l=0}^{\infty}\left(\frac{\lambda}{\omega_b}\right)^l\frac{(-1)^l b^l}{l!} + \text{H.c.} \tag{S13}$$

Under the Stokes resonant condition $\omega_L = \tilde{\omega}_\sigma + n\omega_b$, i.e., $\Delta = \Delta_n(\lambda) = \lambda^2/\omega_b - n\omega_b$, the interaction Hamiltonian Eq. (S13) induces the associated super-Rabi oscillations with n phonons, i.e., $|m, v\rangle \leftrightarrow |m+n, c\rangle$ (with $m = 0, 1, 2, \dots$) By expanding the exponent term containing the ladder operators to the nth-order, one can obtain the effective super-Rabi frequency as

$$\begin{aligned}\Omega_{\text{eff}}^{(n)} =& \Omega |\langle m+n| \exp\left[(\lambda/\omega_b)\left(b^\dagger - b\right)\right] |m\rangle| \\ =& \Omega \exp\left[-\frac{1}{2}\left(\frac{\lambda}{\omega_b}\right)^2\right]\left(\frac{\lambda}{\omega_b}\right)^n \sqrt{\frac{m!}{(m+n)!}} L_m^n((\lambda/\omega_b)^2),\end{aligned} \tag{S14}$$

where $L_m^n(\varepsilon)$ is an associated Laguerre polynomial

$$L_m^n(\varepsilon) = \sum_{j=0}^{m} (-1)^j C_{m-j}^{m+n} \frac{\varepsilon^j}{j!}. \tag{S15}$$

In the main text, we consider the oscillations between the ground state and the excited state with n phonons, i.e., $|0, v\rangle \leftrightarrow |n, c\rangle$. In this case, the effective super-Rabi frequency is simply given by

$$\Omega_{\text{eff}}^{(n)} = \exp\left[-\frac{1}{2}\left(\frac{\lambda}{\omega_b}\right)^2\right]\left(\frac{\lambda}{\omega_b}\right)^n \frac{\Omega}{\sqrt{n!}}. \tag{S16}$$

Strong-driving regime

In the parameter regime $\Omega \sim \omega_b$, the strong driving laser dresses the QD, and the system forms new eigenstates that are a quantum superposition of the bare states. The subsystem Hamiltonian for the strongly driven QD is then

$$H_\sigma = \Delta\sigma^\dagger\sigma + \Omega\left(\sigma + \sigma^\dagger\right), \tag{S17}$$

with eigenstates

$$|+\rangle = c_+|v\rangle + c_-|c\rangle, \tag{S18a}$$
$$|-\rangle = c_-|v\rangle - c_+|c\rangle, \tag{S18b}$$

and corresponding eigenvalues $E_{|\pm\rangle} = \left(\Delta \pm \sqrt{\Delta^2 + 4\Omega^2}\right)/2$, where

$$c_\pm = \sqrt{\frac{2\Omega^2}{\Delta^2 + 4\Omega^2 \pm \Delta\sqrt{\Delta^2 + 4\Omega^2}}} \tag{S19}$$

and $c_+^2 + c_-^2 = 1$. Together with the phonon mode and ignoring the influence of electron-phonon interactions, the eigenvalues become $E_{|n,\pm\rangle} = n\omega_b + \left(\Delta \pm \sqrt{\Delta^2 + 4\Omega^2}\right)/2$. By setting $E_{|0,+\rangle} = E_{|n,-\rangle}$, the n-phonon assisted Stokes resonance $\Delta = \Delta_n(\Omega) = -\sqrt{(n\omega_b)^2 - 4\Omega^2}$ is obtained. In other words, these two states $|0,+\rangle$ and $|n,-\rangle$ are degenerate, when the QD is driven at a n-phonon resonance. We can also derive the effective coupling between the states $|0,+\rangle$ and $|n,-\rangle$ by perturbation theory. Specifically, we write the Hamiltonian in the Hilbert space spanned by the $2n$ ($n > 2$) dressed states $\{|0,+\rangle, |1,-\rangle, |1,+\rangle, \cdots, |n-1,-\rangle, |n-1,+\rangle, |n,-\rangle\}$. This yields a matrix similar to Eq. (S3), but in a frame rotating with frequency $E_{|+\rangle}$, with

$$H^{(n)} = \begin{pmatrix} H^{(n-1)} & V^{(n)T} \\ V^{(n)} & X^{(n)} \end{pmatrix}, \tag{S20}$$

where

$$V^{(n)} = \begin{pmatrix} 0 & \dots & -\sqrt{n-1}c_+c_-\lambda & \sqrt{n-1}c_-^2\lambda & 0 \\ 0 & \dots & 0 & 0 & \sqrt{n}c_+^2\lambda \end{pmatrix}, \quad X^{(n)} = \begin{pmatrix} (n-1)\omega_b & -\sqrt{n}c_+c_-\lambda \\ -\sqrt{n}c_+c_-\lambda & n\omega_b - r \end{pmatrix}, \tag{S21}$$

and $r=\sqrt{4\Omega^2+\Delta^2}$. Here the lowest-order matrix $H^{(2)}$ reads

$$H^{(2)}=\begin{pmatrix} 0 & -c_+c_-\lambda & c_-^2\lambda & 0 \\ -c_+c_-\lambda & \omega_b-r & 0 & \sqrt{2}c_+^2\lambda \\ c_-^2\lambda & 0 & \omega_b & -\sqrt{2}c_+c_-\lambda \\ 0 & \sqrt{2}c_+^2\lambda & -\sqrt{2}c_+c_-\lambda & 2\omega_b-r \end{pmatrix}. \tag{S22}$$

To safely isolate the reduced Hamiltonian $H^{(n)}$ in the truncated Hilbert space spanned by $\{|0,+\rangle, |n,-\rangle, |n-1,+\rangle, |n-1,-\rangle\}$, a series of basic matrix operations are applied into Eq. (S20), and its sub-matrices $V^{(n)}$ and $X^{(n)}$ become

$$V^{(n)}=\begin{pmatrix} 0 & 0 & \dots & 0 & \frac{c_-}{c_+}[(n-1)\omega_b-r] \\ 0 & 0 & \dots & 0 & \sqrt{n}c_+^2\lambda \end{pmatrix}, \quad X^{(n)}=\begin{pmatrix} \left(\frac{c_-}{c_+}\right)^2[(n-1)\omega_b-r]+(n-1)\omega_b & 0 \\ 0 & n\omega_b-r \end{pmatrix}. \tag{S23}$$

Correspondingly, the lowest order matrix $H^{(2)}$ becomes

$$H^{(2)}=\begin{pmatrix} 0 & -c_+c_-\lambda & 0 & 0 \\ -c_+c_-\lambda & \omega_b-r & \frac{c_-}{c_+}(\omega_b-r) & \sqrt{2}c_+^2\lambda \\ 0 & \frac{c_-}{c_+}(\omega_b-r) & \left(\frac{c_-}{c_+}\right)^2(\omega_b-r)+\omega_b & 0 \\ 0 & \sqrt{2}c_+^2\lambda & 0 & 2\omega_b-r \end{pmatrix}. \tag{S24}$$

By applying matrix perturbation theory, i.e., (S6), the effective coupling between the states $|0,+\rangle$ and $|2,-\rangle$ is found as

$$\Omega_{\text{eff}}^{(2)}=\frac{-\sqrt{2}c_+c_-\lambda^2(\omega_b-c_-^2r)}{\omega_b(r-\omega_b)}. \tag{S25}$$

Now, the expression for any order of the effective super-Rabi frequency $\Omega_{\text{eff}}^{(n)}$ can be derived by the method used in the low driving regime. We first consider the truncated Hilbert space spanned by the product states $\{|0,+\rangle, |n,-\rangle, |n-1,+\rangle, |n-1,-\rangle\}$, where the reduced Hamiltonian reads

$$H^{(n)}=\begin{pmatrix} 0 & 0 & 0 & \Omega_{\text{eff}}^{(n-1)} \\ 0 & n\omega_b-r & 0 & \sqrt{n}c_+^2\lambda \\ 0 & 0 & \left(\frac{c_-}{c_+}\right)^2[(n-1)\omega_b-r]+(n-1)\omega_b & \frac{c_-}{c_+}[(n-1)\omega_b-r] \\ \Omega_{\text{eff}}^{(n-1)} & \sqrt{n}c_+^2\lambda & \frac{c_-}{c_+}[(n-1)\omega_b-r] & (n-1)\omega_b-r \end{pmatrix}, \tag{S26}$$

with $\Omega_{\text{eff}}^{(n-1)}$ the effective coupling between the states $|0,+\rangle$ and $|n-1,-\rangle$. Then we can obtain the effective n-phonon super-Rabi frequency $\Omega_{\text{eff}}^{(n)}$, by applying matrix perturbation theory, i.e., (S6), with

$$\Omega_{\text{eff}}^{(n)}=\frac{\sqrt{n}\lambda[(n-1)\omega_b-c_-^2r]}{(n-1)\omega_b[r-(n-1)\omega_b]}\Omega_{\text{eff}}^{(n-1)}. \tag{S27}$$

Following the same procedure, we obtain

$$\Omega_{\text{eff}}^{(n-1)}=\frac{\sqrt{n-1}\lambda[(n-2)\omega_b-c_-^2r]}{(n-2)\omega_b[r-(n-2)\omega_b]}\Omega_{\text{eff}}^{(n-2)}=\frac{\sqrt{n-1}\lambda[(n-2)\omega_b-c_-^2r]}{(n-2)\omega_b[r-(n-2)\omega_b]}\cdots\frac{\sqrt{3}\lambda(2\omega_b-c_-^2r)\Omega_{\text{eff}}^{(2)}}{2\omega_b(r-2\omega_b)}\Omega_{\text{eff}}^{(2)}. \tag{S28}$$

Thus the effective super-Rabi frequency at the n-phonon resonance, i.e., $\Delta=\Delta_n(\Omega)=-\sqrt{(n\omega_b)^2-4\Omega^2}$, can be given by

$$\Omega_{\text{eff}}^{(n)}=(-1)^n\left(\frac{\lambda}{\omega_b}\right)^n\frac{\Omega}{(n-1)!\sqrt{n!}}\prod_{k=1}^{n-1}(nc_-^2-k). \tag{S29}$$

In the main text, it is shown that $\Omega_{\text{eff}}^{(n)}$ agrees with exact numerical simulations in all three regimes. Here as well, one gets the good approximation for the phonon population probability $P_n\approx P_{n-}$. Moreover, from the precise forms of $\Omega_{\text{eff}}^{(n)}$, we show how in the three different regimes $\Omega_{\text{eff}}^{(n)}$ tends to zero as the number of phonons n goes to infinity. The corresponding scaling for the first and second regimes is $1/\sqrt{n!}$, and an additional item $1/(n-1)!$ is added for the case of the third regime.

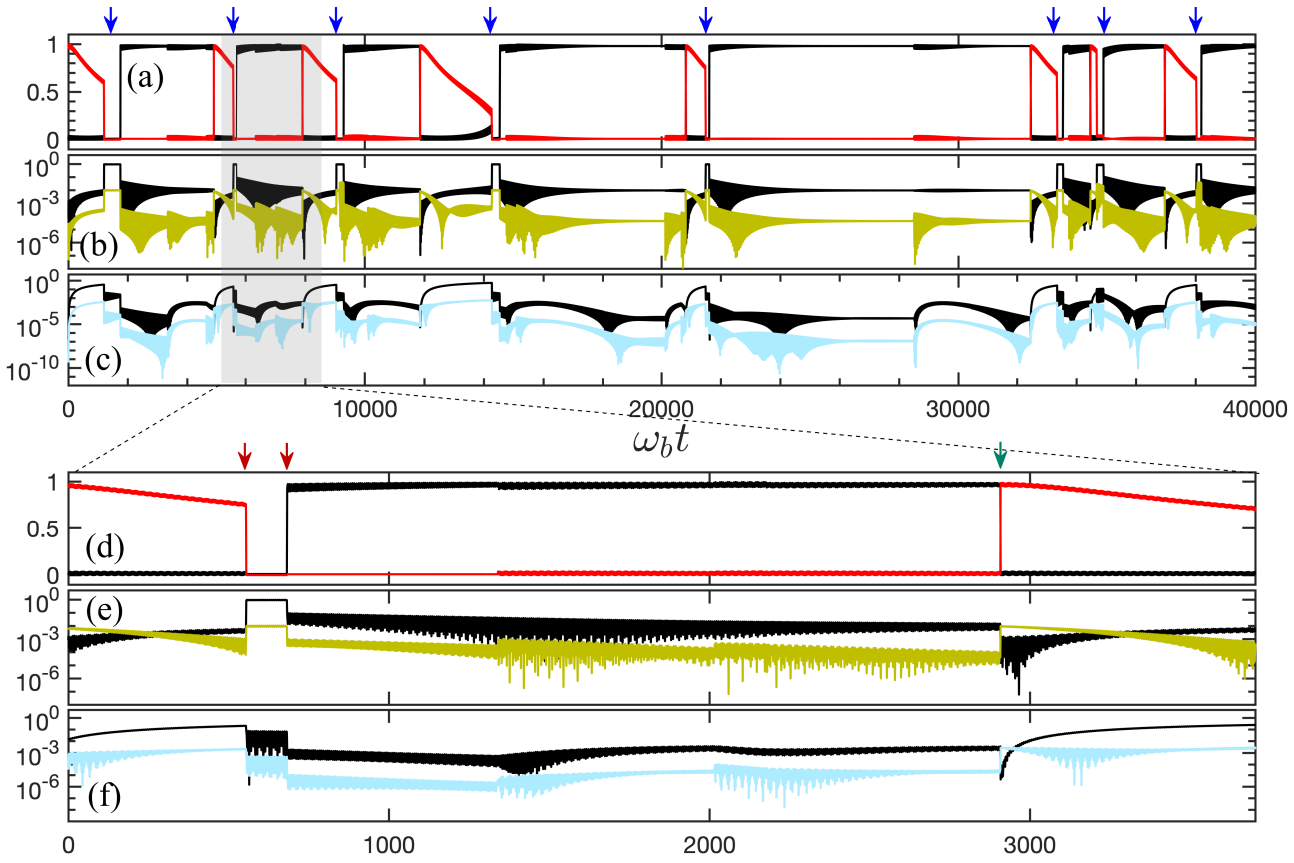

FIG. S1: Quantum trajectory in the two-phonon emission regime for a long-time range (top), with a shaded area zoomed-in to single-out one emission event (bottom). Blue arrows indicate two-phonon bundle emissions. Red arrows in the bottom panel indicate single-phonon emissions, and the green arrow indicates the direct photon emission from the QD flip. The system parameters are the same as in Figs.4(a–c) of the main text.

QUANTUM TRAJECTORIES OF TWO- AND THREE-PHONON BUNDLE EMISSIONS

In the main text, a focus on two-phonon bundle emission is provided as a quantum trajectory in Figs. 4(a–c). This is a very short fraction of the full quantum trajectory, of which a longer portion is shown in the top of Fig. S1. The two-phonon emission events are indicated by blue arrows. The bottom of Fig. S1 is the enlarged region of the shadowed window on the top trajectory, which is the same as Figs. 4(a–c) of the main text. The first red arrow indicates the first phonon emission triggered by the system dissipation, as the system wave function collapses into the one-phonon state with almost unit probability. The system then emits the second phonon during the cavity lifetime, indicated by the second red arrow. Such two emitted phonons are thus released during a very short temporal window, smaller than the cavity lifetime. After the two-phonon emission, the system returns to the vacuum state immediately. The two-phonon state is constructed again after a direct *photon* emission from the QD flip, indicated by the green arrow. In the next cycle, the system undergoes the same cascade emission of phonon pair, each accompanied by a single *photon* emission, which can be used for heralding purposes (e.g., with a delay line).

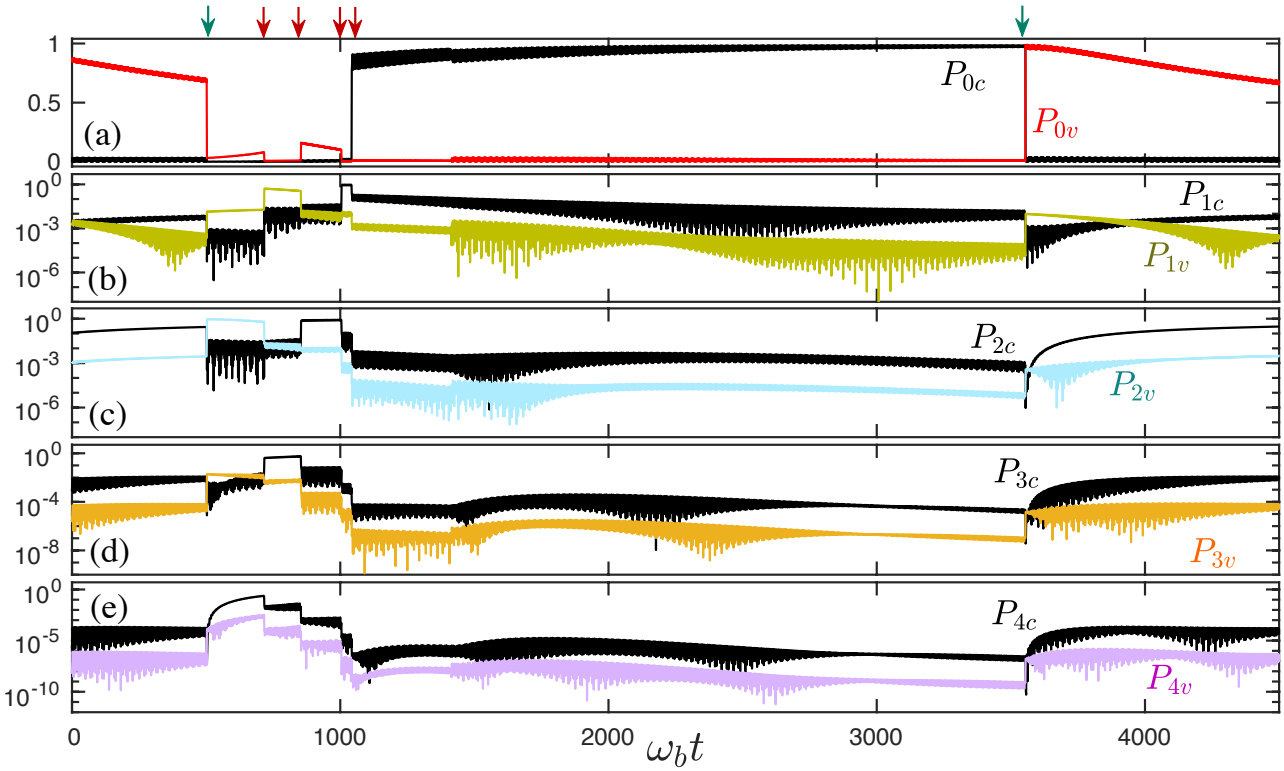

FIG. S2: (a–e) Small fraction of a quantum trajectory featuring two closely-spaced n-phonon emissions at the two-phonon resonance, where $n = 2$, where the QD flips before the first phonon is emitted. Green arrows indicate the direct photon emission from the QD flip, and the red arrows indicate single-phonon emissions. The system parameters are the same as in Fig. S1.

There also exists the possibility for an accidental two 2-phonon bundle emission under the condition of two-phonon resonance, whereby two bundles occur in a so-close time-interval as to be considered simultaneous (four-phonon state for $n = 2$). This harms the purity of n-phonon emission in the same way as successive single-photon emissions spoil the single-photon character of a single-photon source. We show here a single 2×2-phonon bundle emission in Figs. S2(a–e). This phonon emission process is different from the normal n-phonon bundle emissions. Initially, the two-phonon state is still exceedingly occupied with probability close to 30%. Instead of the emission of the first phonon, a flip occurs in the QD, i.e., $|2, c\rangle \rightarrow |2, v\rangle$, and emits a single photon. Due to the continuous laser pumping, the occurrence of new Rabi oscillations between the states $|2, v\rangle$ and $|4, c\rangle$ leads to the result that the four-phonon state is increasingly occupied. Then the system continuously emits the first, second, third and fourth phonons in a very short temporal window triggered by the dissipation of cavity. After the emission of such four phonons, the system returns to the phonon-vacuum state immediately, and the two-phonon state is constructed again after a direct photon emission from the QD flip. Such a 2×2-phonon bundle emission occurring in the regime of two-phonon bundle emission would reduce the purity of the emitted bundle. However, our system can be brought in a regime of phonon-bundle antibunching, i.e., suppressing such close emission of successive bundles. Indeed, through direct computations, we find that this 2×2-phonon bundle emission is hardly found in the two-phonon resonance regime, and only has a probability close to 1% during the full phonon-emission process (see the insert bar graphs in Fig. 4(a) of the main text). It is thus negligible in the parameter regime that we have chosen and could be further optimized.

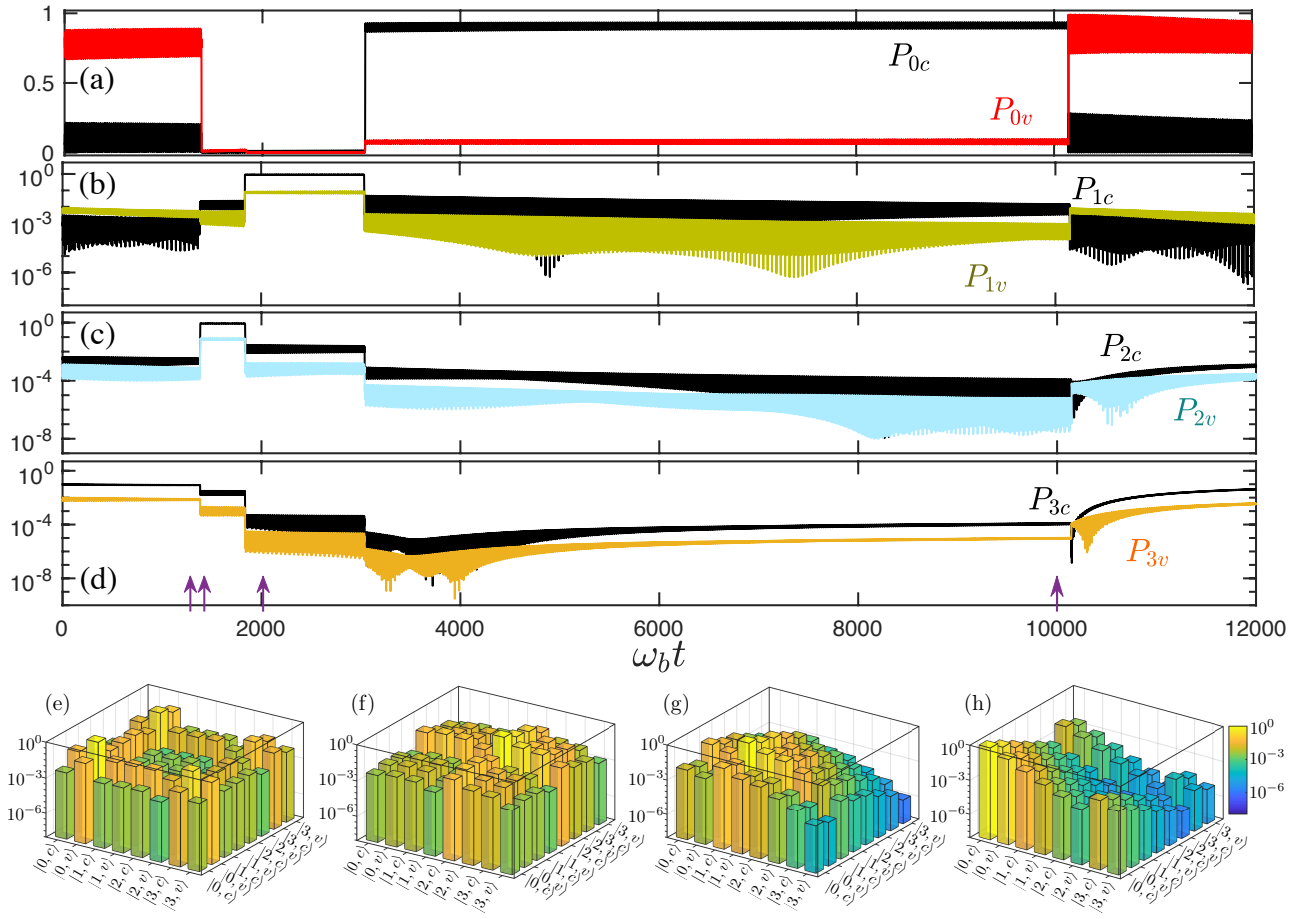

FIG. S3: (a–d) Small fraction of a quantum trajectory in the regime of three-phonon emission. (e–h) The full density matrices of the system at the times indicated by purple arrows, showing the cascaded emission process. The system parameters are $\Omega/\omega_b = 0.8$, $\lambda/\omega_b = 0.1$, $\kappa/\omega_b = \gamma_\phi/\omega_b = 0.0004$, and $\gamma/\omega_b = 0.0002$.

In Figs. S3(a–d), we also show a single three-phonon emission process. The three-phonon state is initially occupied with probability close to 10% thanks to the Stokes resonance, which, similarly to the two-phonon emission process, leads to an actual three-phonon emission. The system dissipation triggers the emission of a first phonon, which collapses the system onto the two-phonon state with almost unit probability. The system then emits the second and third phonons according to the above scenario. This results in the emission of three strongly-correlated phonons, released in a very short temporal window. After the emission of the three phonons, the system returns to the vacuum state immediately, and after the direct *photon* emission from the QD flip, i.e., $|0, c\rangle \to |0, v\rangle$, the three-phonon state is being constructed again to prepare the next three-phonon emission cycle. Figures S3(e–h) show the full density matrices of the system at different times, revealing the intrinsic temporal structure during the three-phonon emission. At first, the system is approximately in a quantum superposition of the states $|0, v\rangle$ and $|3, c\rangle$. Then it undergoes a rapid cascade emission through the Fock states $|n_i\rangle$ $(0 \leq n_i \leq 3)$ in a very short time window. The result *outside* of the cavity of the Fock state initially *inside* is the phonon bundle.

PURITIES OF HIGH-ORDER N-PHONON BUNDLE EMISSIONS

Figure 5 of the main text shows the influence of off-resonance phonon emission on the purities of two- and three-phonon emissions. Figure S4 shows the purities for higher orders, namely, up to five-phonon emission. As expected, the purity is less robust for larger n and requires stronger electron-phonon coupling strengths λ and smaller decay rates κ. However, in our proposal, increasing ω_b can also allow to conveniently reach such parameter-ranges of high purities. In fact, close to 95% four-phonon and close to 80% five-phonon emission are already within reach of feasible experimental parameters ($\omega_b/2\pi = 1\,\mathrm{THz}$, $\omega_\sigma/2\pi = 100\,\mathrm{THz}$, $\Omega/2\pi = 0.2\,\mathrm{THz}$, $\lambda/2\pi = 0.14\,\mathrm{THz}$,

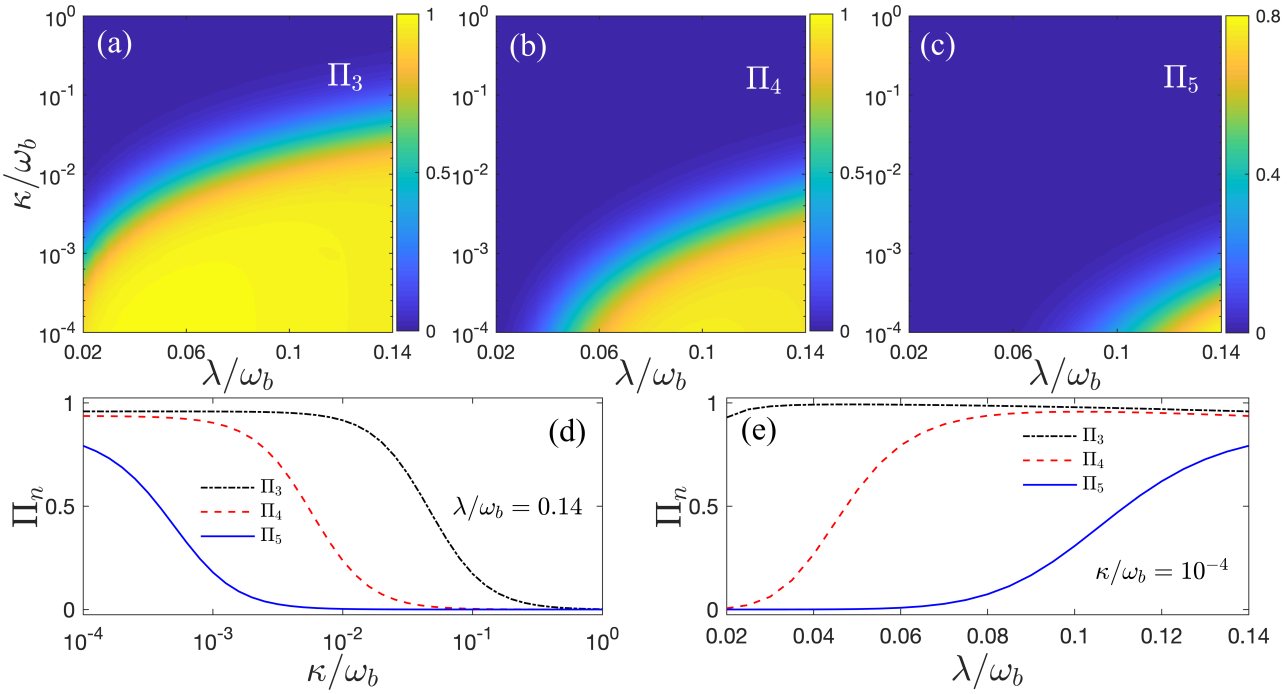

FIG. S4: Purities of (a) three-phonon, (b) four-phonon, and (c) five-phonon emissions versus λ/ω_b and κ/ω_b when the system is driven at the corresponding n phonon resonances. (d–e) The purities along the lines of $\lambda/\omega_b = 0.14$ and $\kappa/\omega_b = 10^{-4}$ in panels (a–c). The system parameters used are $\Omega/\omega_b = 0.2$, $\gamma/\omega_b = 0.0002$ and $\gamma_\phi/\omega_b = 0.0004$.

$\kappa/2\pi = 0.1\,\mathrm{GHz}$, $\gamma/2\pi = 0.2\,\mathrm{GHz}$ and $\gamma_\phi/2\pi = 0.4\,\mathrm{GHz}$) [4–7].

EFFECT OF PURE DEPHASING AND OPTIMUM OF N-PHONON EMISSION

In any realistic physical system, various couplings to the environment ultimately lead to the dephasing of the quantum coherence. This effect for the QD can be described through a Lindblad-type master equation as shown in the main text, i.e., $d\rho/dt = -i[H,\rho] + \kappa\mathcal{L}[b] + \gamma\mathcal{L}[\sigma] + \gamma_\phi\mathcal{L}[\sigma^\dagger\sigma]$, where $\mathcal{L}[O] = (2O\rho O^\dagger - \rho O^\dagger O - O^\dagger O\rho)/2$, with κ (γ) the cavity (QD) decay rate, and γ_ϕ the rate of pure dephasing of the QD. Figure 4 of the main text shows a quantum trajectory of two-phonon bundle emission where the effect of pure dephasing of the QD is taken into account. We find that the two-phonon emission in a rapid cascade is not disrupted by the presence of pure dephasing, since the whole cascade emission of phonon pair occurs in a very small time window. In Fig. S5(a), we show the effect of γ_ϕ on the purities of two- and three-phonon bundle emissions, which demonstrates that the scheme is robust to pure dephasing of the QD, and that bundle emission gets significantly disrupted only when γ_ϕ becomes large. Indeed, pure dephasing merely harms the QD and has no direct influence on the cavity, but pure bundle emission occurs precisely through the cavity and pure dephasing is only a cause of impediment for building the n-phonon state due to the decoherence, but this merely slows down the rate. Once the system collapsed in the n-phonon state, the cascade-emission process is essentially shielded from the pure dephasing of the QD.

In the quantum trajectories, the buildup of the n-phonon state and the cascade emission of phonons are related to the effective Rabi frequency $\Omega_{\mathrm{eff}}^{(n)}$ and the phonon relaxation rate κ, respectively. If the value of κ is much larger, the detection of emitted phonons can lead to a quantum Zeno dynamics, freezing out the oscillations. If, on the other hand, the Rabi frequency $\Omega_{\mathrm{eff}}^{(n)}$ was much larger, the system would exhibit many oscillations before emitting a phonon. The competition between the above two processes ultimately leads to the optimal bundle emission with high purity. In Fig. S5(b), we thus calculate numerically the influence of the effective two-phonon Rabi frequency on the purity of two-phonon emission for different phonon relaxation rates κ. A sweet spot is obtained by optimizing between these two processes, and is given by $\kappa \approx 10\Omega_{\mathrm{eff}}^{(2)}$. Figure S5(b) also shows that there exists a relatively wide range around this sweet spot, where one can obtain bundle emissions with high purity.

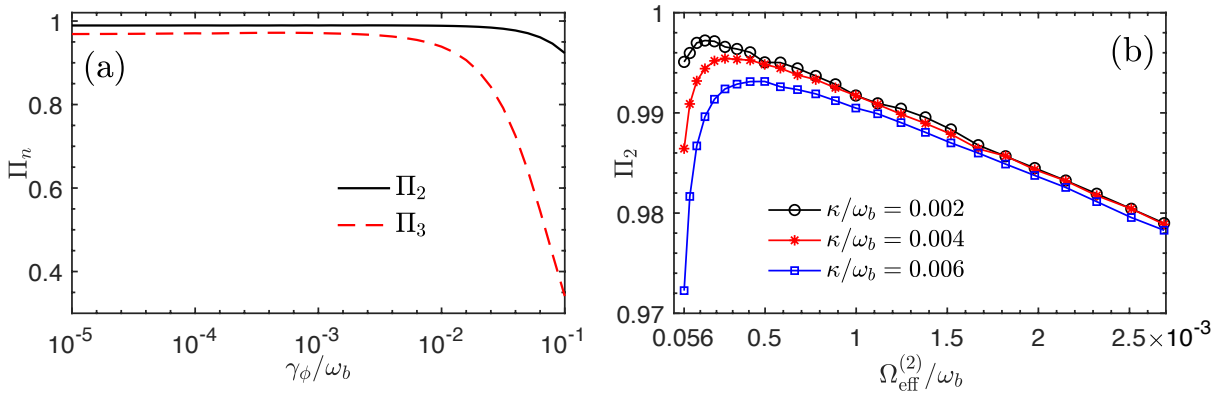

FIG. S5: (a) Effect of the pure dephasing γ_ϕ of the QD on the purities of two- and three-phonon emissions. (b) Purity of two-phonon emission as a function of the effective two-phonon Rabi frequency $\Omega^{(2)}_{\rm eff}$ for different rates of cavity decay κ/ω_b. The system parameters used are $\Omega/\omega_b = 0.2$, $\lambda/\omega_b = 0.1$, $\gamma/\omega_b = 0.0002$, (a) $\kappa/\omega_b = 0.002$ and (b) $\gamma_\phi/\omega_b = 0.0004$.

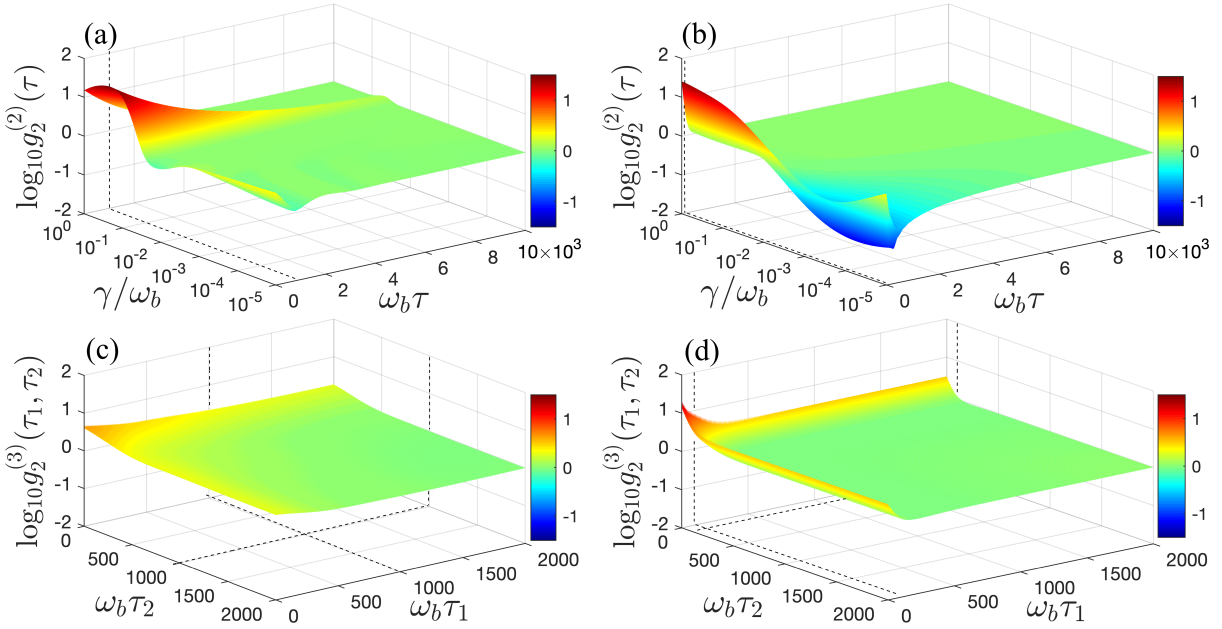

FIG. S6: (a)-(b) Second-order two-phonon correlations $g_2^{(2)}(\tau)$ versus QD decay γ/ω_b for different cavity decays κ/ω_b. With increasing γ/ω_b, the emitted two-phonon bundles evolve from bundle antibunching to bunching, passing thorough the no-correlation regime (at (a) $\gamma/\omega_b = 0.0006$ and (b) $\gamma/\omega_b = 0.009$). (c–d) Third-order phonon correlations $g_2^{(3)}(\tau_1,\tau_2)$ of the two-phonon bundle statistics when $\gamma/\omega_b = 0.0006$ and $\gamma/\omega_b = 0.009$ for different values of κ/ω_b. The dashed lines in all panels correspond to $\tau = 1/\kappa$ or $\tau_i = 1/\kappa$ $(i = 1, 2)$. The system parameters are $\Omega/\omega_b = 0.2$, $\lambda/\omega_b = 0.1$, $\gamma_\phi/\omega_b = 0.0004$; and $\kappa/\omega_b = 0.001$ for (a) and (c), $\kappa/\omega_b = 0.01$ for (b) and (d), and the two-phonon associated Stokes resonance has been chosen.

CORRELATIONS OF THE EMITTED n-PHONON BUNDLES

Standard correlation functions $g^{(n)}$ apply to phonons rather than to bundles, for which it is more appropriate to use the m-bundle correlation functions $g_m^{(n)}$ [8, 9] that quantify nth-order correlations of m-phonon bundles:

$$g_m^{(n)}(t_1,...,t_n) = \frac{\langle \mathcal{T}_-\{\prod_{i=1}^n b^{\dagger m}(t_i)\}\mathcal{T}_+\{\prod_{i=1}^n b^m(t_i)\}\rangle}{\prod_{i=1}^n \langle b^{\dagger m} b^m\rangle(t_i)}, \tag{S30}$$

where $\mathcal{T}_\pm$ represents the time-ordering operators. Note that the standard correlation functions are the particular case $m = 1$ of these quantities. Figure S6 shows the two- (upper row) and three- (lower row) order correlations of

two-phonon bundle emisssion for two-cavity decay rates κ (left and right columns), the corresponding correlations can be given by

$$g_2^{(2)}(\tau) = \frac{\langle b^{\dagger 2}(0) b^{\dagger 2}(\tau) b^2(\tau) b^2(0)\rangle}{\langle (b^{\dagger 2} b^2)(0)\rangle \langle (b^{\dagger 2} b^2)(\tau)\rangle}\,, \tag{S31a}$$

$$g_2^{(3)}(\tau_1,\tau_2) = \frac{\langle b^{\dagger 2}(0) b^{\dagger 2}(\tau_1) b^{\dagger 2}(\tau_2) b^2(\tau_2) b^2(\tau_1) b^2(0)\rangle}{\langle b^{\dagger 2} b^2(0)\rangle \langle b^{\dagger 2} b^2(\tau_1)\rangle \langle b^{\dagger 2} b^2(\tau_2)\rangle}\,, \tag{S31b}$$

where τ and τ_i $(i = 1, 2)$ are the time delays between successive phonons. For the two-phonon bundle correlations, during the valid range of $g_2^{(2)}(\tau)$ (i.e., $\tau > 1/\kappa$), we show how the QD decay rate γ/ω_b can tune the bundle statistics $g_2^{(2)}(\tau)$ from antibunching to bunching, passing by the Poissonian case of no bundle-correlations with $g_2^{(2)}(\tau) = 1$. The bundle antibunching, possibly the case of most interest for further quantum processing of the emission, is obtained with short-lived cavities—to release the bundles quickly—coupled to long-lived QD excitations, to separate the successive emission events. The Poissonian case corresponds, according to Glauber's theory of quantum coherence, to a coherent state of phonon bundles, provided that this occurs to all orders. We show that this holds indeed at the next, third-order correlation, with $g_2^{(3)}(\tau_1, \tau_2)$ of the two-phonon bundle in Figs. S6(c–d). Except in the small-time windows of width κ^{-1} centered on zero, where the bundle-correlation function is ill-defined (as such short times probe inside the bundle itself), the third-order correlation functions in the sought coherent regime indeed satisfy $g_2^{(3)}(\tau_1, \tau_2) \approx 1$. This supports a regime of two-phonon bundles coherent states emission with the bundles uncorrelating from our device (i.e., the two-phonon laser), that also operates in other regimes as a thermal source of phonon bundles with the bundles bunching or on the opposite limit as a single-bundle emitter with the bundles antibunching (i.e., the two-phonon gun).

* Electronic address: xinyoulu@hust.edu.cn
† Electronic address: yingwu2@126.com

[1] K. K. W. Ma and C. K. Law, Three-photon resonance and adiabatic passage in the large-detuning Rabi model, Phys. Rev. A. **92**, 023842 (2015).
[2] C. S. Muñoz, F. P. Laussy, E. del Valle, C. Tejedor, and A. González-Tudela, Filtering multiphoton emission from state-ofthe-art cavity quantum electrodynamics, Optica **5**, 14-26 (2018).
[3] C. A. Blockley, D. F. Walls, and H. Risken, Quantum Collapses and Revivals in a Quantized Trap, Europhys. Lett. **17**, 509 (1992).
[4] P. Borri, W. Langbein, S. Schneider, and U. Woggon, Ultralong Dephasing Time in InGaAs Quantum Dots, Phys. Rev. Lett. **87**, 157401 (2001).
[5] E. M. Weig, R. H. Blick, T. Brandes, J. Kirschbaum, W.Wegscheider, M. Bichler, and J. P. Kotthaus, Single-Electron-Phonon Interaction in a Suspended Quantum Dot Phonon Cavity, Phys. Rev. Lett. **92**, 046804 (2004).
[6] G. Rozas, M. F. P.Winter, B. Jusserand, A. Fainstein, B. Perrin, E. Semenova, and A. Lemaître, Lifetime of THz Acoustic Nanocavity Modes, Phys. Rev. Lett. **102**, 015502 (2009).
[7] E. Stock, M.-R. Dachner, T. Warming, A. Schliwa, A. Lochmann, A. Hoffmann, A. I. Toropov, A. K. Bakarov, I. A. Derebezov, M. Richter, V. A. Haisler, A. Knorr, and D. Bimberg, Acoustic and optical phonon scattering in a single In(Ga)As quantum dot, Phys. Rev. B **93**, 041304 (2011).
[8] C. S. Muñoz, E. del Valle, A. G. Tudela, K. Müller, S. Lichtmannecker, M. Kaniber, C. Tejedor, J. Finley, and F. Laussy, Emitters of N-photon bundles, Nat. Photonics **8**, 550 (2014).
[9] Y. Chang, A. González-Tudela, C. S. Muñoz, C. Navarrete-Benlloch, and T. Shi, Deterministic Down-Converter and Continuous Photon-Pair Source within the Bad-Cavity Limit, Phys. Rev. Lett. **117**, 203602 (2016).